Cinematic Characteristics of Amazonian convective systems

Evandro M. Anselmo[1,2,3], **Luiz A. T. Machado**[1], **Courtney Schumacher**[2]

[1]National Institute for Space Research, São José dos Campos, Brazil
[2]Texas A&M University, College Station, Texas, USA
[3]CAPES Foundation, Ministry of Education of Brazil, Brasília, Brazil

Corresponding author: Evandro M. Anselmo, evandromoimaz@gmail.com

Abstract

A convective system tracking was made using the GOES-13 (10.2–11.2 μm) infrared imagery between 13°N–15°S and 82°–34°W covering the entire Amazon rainforest region during 2014 and 2015, same period of GoAmazon2014/5 field campaign. Despite the path travelled by convective systems covers an area, previous studies accounted the cloud clusters positions as points (geometric center), the trajectories as lines, and selecting just those systems with spontaneous initiation and dissipation by simple decay. In this research all Amazonian convective systems were evaluated and its trajectories were defined as the union of cloud clusters areas that defined each system. The cloud clusters tracked had continuous area greater than or equal to 2500 km^2 with cloud top brightness temperature less than or equal to 235 K. An total of 116,701 convective systems were found and the probability of occurrence of track areas, lifetime and systems velocities, as well as the maps of total and seasonal geographic density of trajectories, and the geographic density of clusters at: genesis, three steps of propagation, and dissipation are studied. The coastal and basin systems occurrence had a seasonal dependence, and although the average of systems velocities indicate westward predominant displacements, the probability of meridional velocities was practically the same for northward or southward and 35% of zonal velocities were associated with eastward movement.

1 Introduction

A predominant easterly propagation of Amazonian convective systems has been showed based on the average of systems velocities gridded over Amazon basin [*Machado et al.*, 1998; *Rehbein et al.*, 2017]. In addition, others propagation patterns was also observed by *Laurent et al.* [2002] associated with the Easterly and Westerly regimes. *Angelis et al.* [2004] revealed rain bands propagation from the western and eastern Amazon towards its interior, and from western subtropical South America towards the east. They discussed the Andes Effect on the convective system propagations. All these studies are based in short period dataset and/or present an average description of the mesoscale convective systems. Besides the averages trajectories, there is a lack of information describing the trajectories complexity of the Amazon convective systems.

Greco et al. [1990], described the characteristics of convective systems propagation during the Amazon Boundary-Layer Experiment (ABLE 2B). They presented three types of convective system propagation, the coastal occurring systems corresponding to large squall lines formed along the northern coast of Brazil and propagate across the Amazon basin. These systems were also described by *Garstang et al.* [1994] and denominated by Amazon Coastal Squall Lines. The second type was called as basin occurring systems formed in the Central Amazon and propagate to east and finally the locally occurring systems with short life cycle and propagation.

The classification of convective systems as locally, basin and coastal occurring was made generally made visually using geostationary imagery [*Kousky*, 1980; *Greco et al.*, 1990; *Garstang et al.*, 1994; *Cohen et al.*, 1995]. However, sometimes is difficult to follow and describe the dissipation, initiation, merge and split among these different type of systems in the Central Amazon Basin. *Tang et al.* [2016] present case studies of each of these convective systems and discuss that the differentiation between basin and coastal systems occurring is difficult. *Burleyson et al.* [2016] observed that coastal cloudiness from previous day could propagate and arrive in Manaus region in phase with the local diurnal surface heating of following day, making the differentiation between local or non-local convection more complex.

This study employ an automatic tracking algorithm similar to the one used by *Woodley et al.* [1980]; *Williams and Houze Jr* [1987]; *Chen et al.* [1996]; *Machado et al.* [1998]; *Mathon and Laurent* [2001]; *Vila et al.* [2008] to evaluate the convective systems trajectories.

The Cloud tracking was applied using GOES satellite images during the two years of Green Ocean Amazon 2014–2015 (GoAmazon2014/5) field campaign [see *Martin et al.*, 2016, for a detailed description].

Coastal systems has been associated with large amount of precipitation during nighttime where the GoAmazon2014/5 was realized [*Rickenbach*, 2004; *Tang et al.*, 2016] and here we are evaluating the amount of system comings from coast or from basin region using objective tracking.

The main goals of this study is to present a detailed and objective description of the seasonal variation of the geographic density of convective system trajectories over the Amazon Basin. The study describes the density of convective systems during the three lifetime stages, the initiation, mature and dissipation. In addition, a specific analysis is performed for the systems reaching the GoAmazon 2014/15 sites describing its origin. This study provides the convective system speed probability of occurrence and its preferential propagations directions, providing an information that the average propagation information cannot revel.

2 Geostationary infrared imagery and the cloud clusters tracking methodology

The GOES-13 channel 4 (10.2–11.2 μm) infrared imagery was used to track the Amazon convective system. This dataset is stored by the National Institute for Space Research (INPE) every 30 min with 4 km $\times$ 4 km (at nadir) spatial resolution. The study region was defined between 13°N–15°S and 82°–34°W covering northern South America (entire Amazon region) and covered the years 2014 and 2015, the two years of the GoAmazon experiment [*Martin et al.*, 2016, see].

Regions with a continuous area greater than or equal to 2500 km^2 and cloud top brightness temperature (Tb) less than or equal to 235 K were defined as a cloud cluster. The cloud clusters in successive images were compiled to define the full life cycle of convective systems. There are occasional time gaps in the satellite imagery and the maximum time tolerance given for the tracking system to continue the track without start new systems was two consecutive missing images (one and a half hours). However, sometimes the archive had images spaced by 15 minutes that was also considered. Thereby, if we had one image at 00:00 and the next at 1:45, this time gap of 1 h and 45 min is considered as two consecutive missing images, but when we had one image at 00:00 and the next at 2:00, three consecutive missing images were considered.

30,474 images were evaluated in the two years analyzed. During this period there were four time gaps with more than one day (from 1 day to 4 days in one case), 576 gaps of 3 hours, 71 gaps of 2,5 hours, 38 gaps of 2 hours, 76 gaps of 1,5 hour and 643 gaps of 1 hour (one missing image).

The minimum overlap to identify two cloud clusters as the same system at t_0 and at t_0+ dt was fixed in 150 pixels, or approximately 2400 km^2. This value was chosen base on *Vila et al.* [2008], that considering convective systems average speed of 45 km/h and eccentricity equal 0.5, concluded that an overlap larger than 150 pixels is more appropriated for the time (dt = 30 min) and spatial (4 km $\times$ 4 km at nadir) imagery resolution employed in this study.

This kind of tracking can reveal some possible pathways to connect clusters in time and space between the cloud clusters distribution of image at t_0 and of image at t_0+dt. The main possible pathways describes in previous studies are the continuity, merge, and split. Also, can be determined if genesis is a result of new growth or a split from another system or if dissipation results from cloud dissipation or merge into another system as suggested by [*Woodley et al.*, 1980; *Williams and Houze Jr*, 1987; *Mathon and Laurent*, 2001; *Vila et al.*, 2008]. Additionally, continuity, merge, and split pathways can occur simultaneously [*Woodley et al.*, 1980; *Mathon and Laurent*, 2001], and when it occurs the tracking has multiple process of clusters connection.

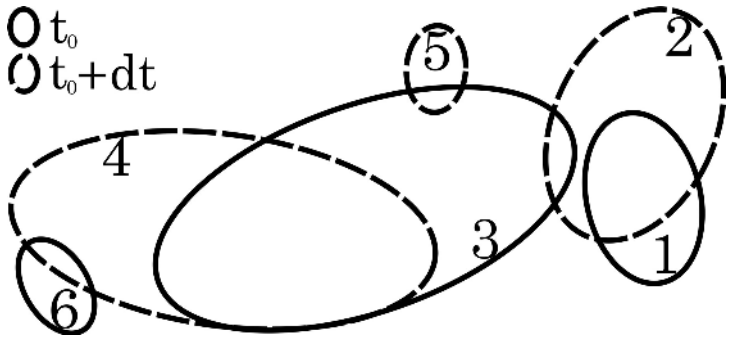

Figure 1. Example of multiple process of cloud cluster connexion: cluster 4 is merge result between the clusters 3 and 6; the clusters 2, 4 and 5 are split from cluster 3; and cluster 2 is merge result between clusters 1 and 3.

Based on our two years data set and our 235K threshold, there were 668,894 instances of clusters overlap to evaluate. Simple continuity represented 83.4% (558,082), mergers represented 5.4% (35,826), splits represented 5.6% (37,578), and multiple processes represented 5.6% (37,408) of the cases. Figure 1 presents an example of multiple process of cloud clusters connexions. Observe that the cluster 4 at t_0+dt, can be considered with merge result between the clusters 3 and 6 at t_0. The clusters 2, 4, and 5 at t_0+dt can be a result of split from cluster 3 at t_0 while the cluster 2 at t_0+dt can be merge result between the clusters 1 and 3 at t_0. Considering the maximum overlapping between these clusters [*Mathon and Laurent*, 2001], we are fairly certain that cluster 1 is connected with cluster 2 and cluster 3 is connected with cluster 4, i.e. there are two valid connexions, and this is the method that we assign when multiple processes were present.

If a multiple process is occurring, we cannot distinguish if the connection between the clusters of image at t_0 and of image at t_0+dt are result of merge, split or simple continuity.

Sometimes we had until 9 valid connections in just one overlap with multiple process, that is to say, until 9 systems travelling side by side. In these cases, the new initiation or spontaneous initiation, can be considered as a result of split (or split generation). For example, the cluster 5 ($t_0 + dt$) could be a candidate to a new system initiation just near to other system. We know by the maximum overlapping criteria that, the clusters 3 at t_0 is clearly connected with cluster 4 at t_0+dt, thereby a cluster in position as the cluster 5 at t_0+dt, can be a new initiation that occurred near to cluster 4 at $t_0 + dt$, mainly in situations when we had one or two missing images due time gaps in satellite imagery database. On account of the valid overlap ($\geqslant$ 150 pixels) between the cluster 5 ($t_0 + dt$) and the cluster 3 (t_0), the cluster 5 is considered with a split generation from cluster 3 (t_0).

Also, a simple decay (dissipation) can be considered as a merging end. We know by the maximum overlapping criteria that, in figure 1 the cluster 1 (t_0) is connected with cluster 2 ($t_0 + dt$) while the cluster 3 (t_0) is connected with cluster 4 ($t_0 + dt$), consequently we have two systems travelling one beside another. If t_0 is the last time step of a third system connected with the cluster 6, this third system can be considered as a merging end because its valid overlap with the cluster 4 (t_0+dt), but the cluster 6 (t_0) also can be just the simple decay of one convective system near to another.

Inside of the 37,408 instances of clusters overlaps associate with multiples processes, there were 73,222 valid connections between cluster at t_0 and t_0+dt, i.e. 10% of the total pathways of connections.

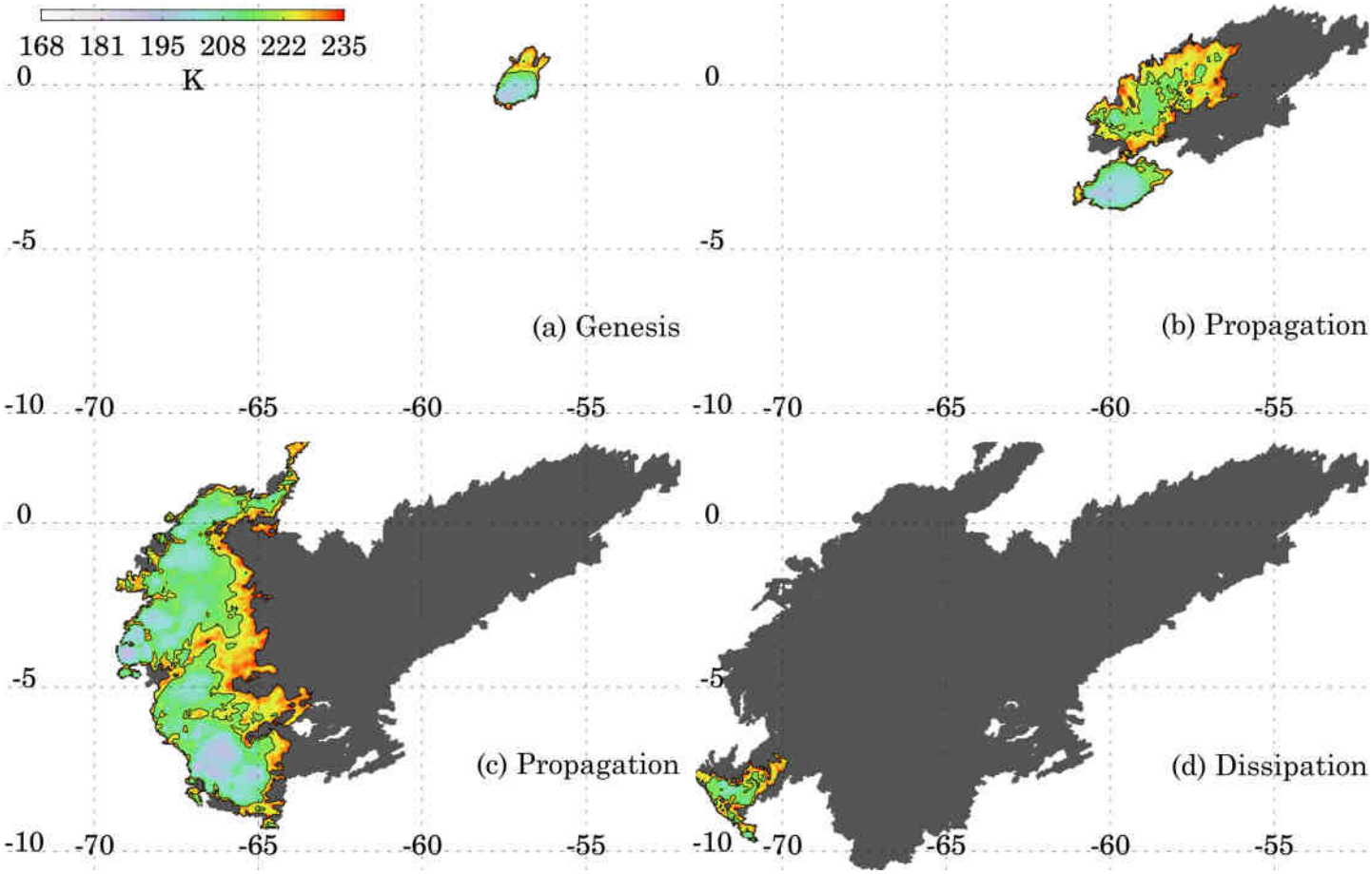

Figure 2. Convective system tracking. (a) shows the genesis at 2014-03-20 00:00, (b) and (c) are the propagation positions at 2014-03-20 12:00 and at 2014-03-21 04:30 respectively, and (d) is the dissipation at 2014-03-21 17:30. The colors describe the infrared brightness temperature and the bidimensional trajectory traveled by the systems is described by the gray contour.

The tracking algorithm employed in this research select all convective systems tracked independent if the geneses are a new initiation, a result of split or if the dissipation was a merging end or simple decay. We are interested in evaluated all tracks, mainly those that form a population of convective systems traveling side by side (in *Houze Jr* [1993], MCS is defined with a "...ensemble of thunderstorms" between others criteria). In *Machado and Laurent* [2004], the selection of just the convective systems with spontaneous initiation and with end by dissipation had the objective to make a nowcasting scheme based on area expansion of these systems and this is not the case in this research.

During the tracking process, we calculate: lifetime, displacement, velocity and the bidimensional trajectory. In previous studies cited here, the trajectories of the systems were represented with a line made by the connection of geometrical center or weighted center of each cloud cluster that defined the system. In this study, the trajectory is not considered as a line. Here, the trajectory represent the union of all cloud clusters areas that defined the system. Figure 2 presents an example illustrating the spatial trajectory of system tracked on 21th March, 2014, the trajectory is the gray area in the image.

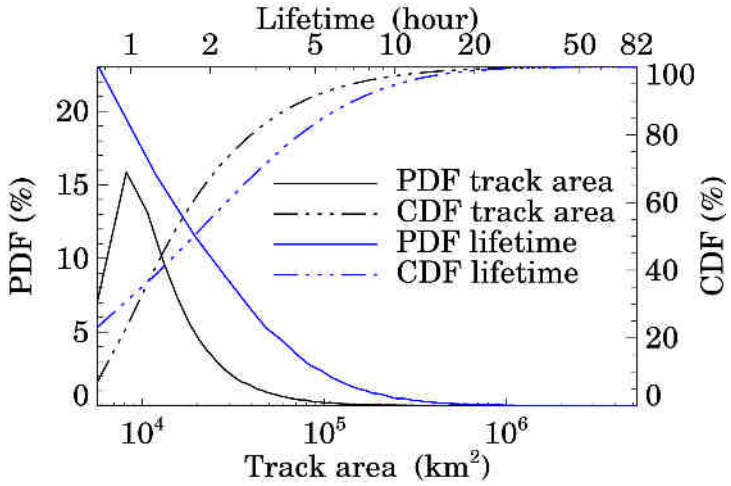

Figure 3. Sample of bidimensional tracks and lifetimes as PDF and CDF for the 116,701 systems.

3 Results

The tracking algorithm found 116,701 convective systems that were connected in at least two consecutive satellite images with a minimal overlapping area of 150 pixels. As already mentioned, GOES-13 imagery is usually provided each 30 min, however, sometimes 15 minutes images intervals were included in the dataset and considered in the tracking.

Figure 3 presents the Probability Distribution Function (PDF) and the Cumulative Distribution Function (CDF) of convective systems tracks areas and lifetimes. The tracks areas and lifetimes were binned in 2500 km^2 and 0.5 h respectively. The most frequent areas are found around 8.2×10^3 km^2, while the median (50th percentile of CDF) was 1.45346×10^4 km^2, the 90th percentile corresponded to an area of 7.68921×10^4 km^2, and the maximum track area was 5.2476340×10^6 km^2. The lifetime decreases exponentially with median lifetime of 1.5 h. In 90th percentile the lifetime was 7 hours, however, there was found the longer lived with 82 hours.

3.1 Geographic density of convective systems trajectories

The trajectories were gridded into a 0.04°×0.04° grid to compute the geographic density of trajectories as the spatial distribution of the percentile of all convective system to cross the region. Figure 4a presents this spatial distribution where values are expressed in percentage (colors) as the number of systems crossing the region normalized by the total number of convective systems tracked (116,701). This Fig. can be interpreted as the probability path of convective systems. One can note a region in the Brazilian coast with high probability and a broader region in Central Amazonia with high probability to have convective systems passing the region. This region, in the Northwest and Central Amazon have probabilities of occurrence between 0.440% and 0.625% (514–729 systems overpass).

The coastal occurrence more frequent between Para and Maranhão have probabilities values between 0.300% and 0.525%. The Amapa, French Guiana, Suriname and Guyana, also on the coast, have smaller probability of around 0.150–0.250%. In South of Amazon River, the trajectories between the coast and the Central Basin were more connected than the North side of Amazon River.

There is a strong gradient of probability of occurrence perpendicular to a Northwest – Southeast line, comprised in 7° S, 48° W and 3° N, 68° W. In two years, there were ≈292 sys-

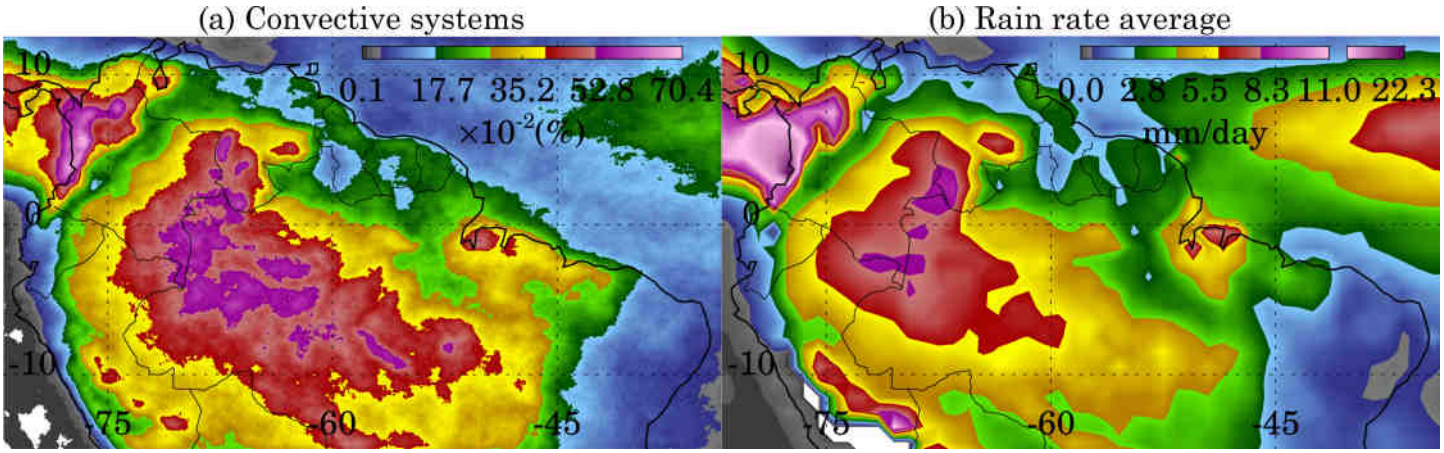

Figure 4. Geographic density of convective systems trajectories with resolution of 0.04° × 0.04° (a) and the TAPEER-BRAIN rain rate average in 1° × 1° (b) during 2014 and 2015.

tems near of this line and ≈200 km westward ≈467 systems. This transition region covers the place where the GoAmazon 2014/15 was held.

In central part of figure 4a, one can note the convection suppression over Madeira, Negro, Amazon, and Tapajos Rivers with the two maximums around 0.600% between: Negro and Amazon Rivers, Madeira and Amazon Rivers and that and that is probably related to the river breeze circulation triggering convection as discussed by *Santos et al.* [2014].

The maxima densities of probability were found over Colombia in extreme North of Andes mountain range with 0.700%. This is a permanent region of convection as discussed by *Horel et al.* [1989]; *Machado et al.* [2004].

Figure 4b presents the rain rate (mm/day) computed by the TAPEER-BRAIN product [*Chambon et al.*, 2012; *Roca et al.*, 2010; *Chambon et al.*, 2013] for same period. As expected, the geographic density of trajectories have a good agreement with the daily accumulated surface rainfall.

The seasonal influence on trajectories can be seen in figure 5. The trajectories during: December, January, February (DJF); March, April, May (MAM); June, July, August (JJA); as well as September, October, November (SON), was gridded separately and the geographic probability density in each season is shown in percentage as presented in the figure 4a.

In general, the movement of trajectory frequency inside the study region present maxima values concentered in South during DJF, East in MAM, North in JJA and West in SON. Figure 5b (MAM) clearly shows the dominant season for the coastal systems between Para and Maranhão coast where is the largest area with the highest values of probability (0.194–0.259%). Additionally, these months (MAM) present high probability of trajectories inside the Central Basin connected to the coast, this is the season where the coastal squall lines propagate further to the Central Basin. In DJF (figure 5a) this connection can also be seen, but the trajectories over coast have smaller probability (≈0.130%) than during MAM (≈0.220%). *Cohen et al.* [1995]; *Alcântara et al.* [2011], show the propagation of Amazon Coastal Squall Lines (ACSL) more frequent during the transition season wet to dry (MAM). During SON (Fig. 5d), the trajectories are quite disconnected from coast indicating the most frequency of the basin occurring systems described in *Greco et al.* [1990]. In JJA the trajectories were further Northern mainly observed close to French Guiana and Amapa coast moving to Central Amazon (figure 5c), but with probability of occurrence lower than 0.098%. Figure 5 clarify the seasonal dependence of the convective system trajectories and numbers of occurrence.

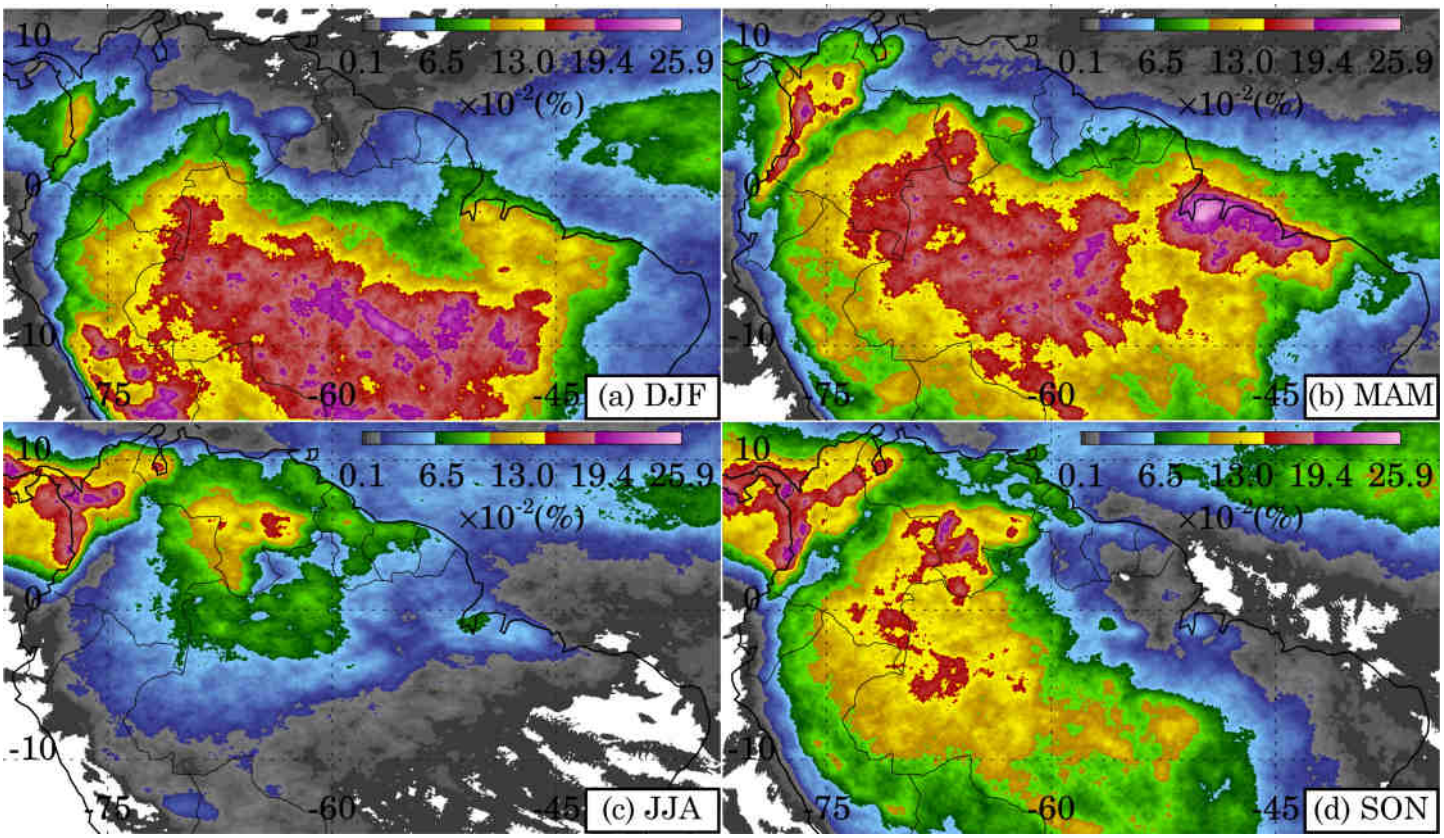

Figure 5. Geographic density of convective systems trajectories for: December, January, February (a); March, April, May (b); June, July, August (c); and, September, October, November (d), of 2014 and 2015.

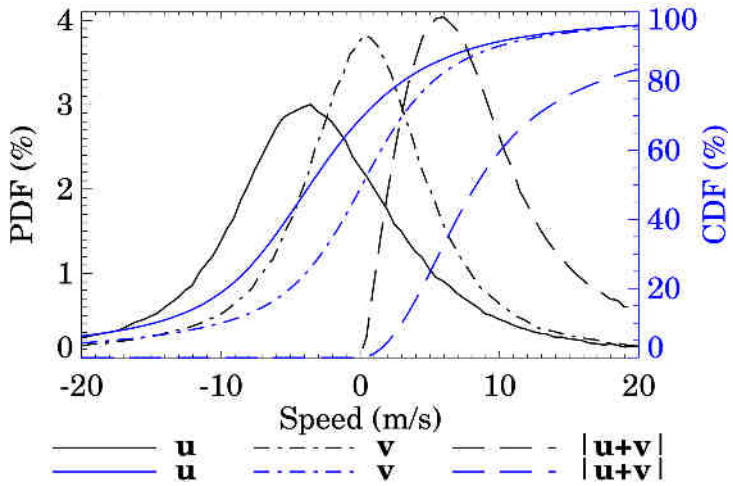

Figure 6. Probability Distribution Function (PDF) and Cumulative Distribution Function (CDF) of velocities: **u**, **v** and, (|**u** + **v**|) for each step of 116,701 systems found.

3.2 Convective systems velocities

Each system life cycle selected has several steps in space-time and for each step is possible to determine the system velocity. For the 116,701 system life cycles selected during the two years, 704,708 system velocities were computed. Each velocity was calculated as the ratio between the displacement vector created by the position of cloud cluster geometric center at t_0 and $t_0 + dt$ and the time interval (dt) between the successive satellite images.

Figure 6 presents the PDF and CDF binned in each 0.5 m/s of the zonal and meridional components **u** (East–West), **v** (North–South), as well as the absolute (|**u** + **v**|) velocity. The highest probability values of **u** sample (2.9%) is −2.8 m/s (westward zonal propagation) and the highest probability values of **v** sample (4.0%) is 0.3 m/s. In an average, the systems traveled predominantly with westward zonal propagation of 2.5 m/s and northward meridional propagation of 0.2 m/s, but when we look for all sample of **u** and **v** in figure 6, the distribution of positives (eastward zonal propagations and northward meridional propagations) and negatives (westward zonal propagations and southward meridional propagations) values are quite symmetric. Here we can see that despite the low-levels and mid-levels flow be predominant in westward, 51% and 49% of **v** components are for northward and southward respectively and the **u** components above the 65th percentile of the CDF are related with positive zonal velocities, showing a group of 35% of sampling with eastward zonal propagation. The system average speed propagation (|**u** + **v**|) is 12.9 m/s, the median (50th percentile of CDF) is 7.9 m/s, and the maximum value registered was 537.5 m/s. The tail of the distribution, presenting these huge velocities cannot be considered as a realistic system displacement velocity, it is probably related to the complexes merges that promote considerable changes in the system geometric center among subsequent cloud clusters.

In addition, the probabilities of convective systems velocities was evaluated regionally every 7° × 8°, accounted values between 1 m/s and 21 m/s binned in 4 m/s and 22.5° of speed and directions respectively in the form of graphics commonly named as wind rose plot, shown in figure 7. The concentric circles indicate the regional probability (5%, 10%, and 15%) in each propagation direction sector and the colors, the convective systems speed classes.

In region between 58° W – 50° W and 6° N – 13° N the westward propagation sector exceeds 15% and reach the maximum value of 21%. The sectors with northeastward, eastward and southeastward convective systems velocities can be seen in all Amazon region totalizing

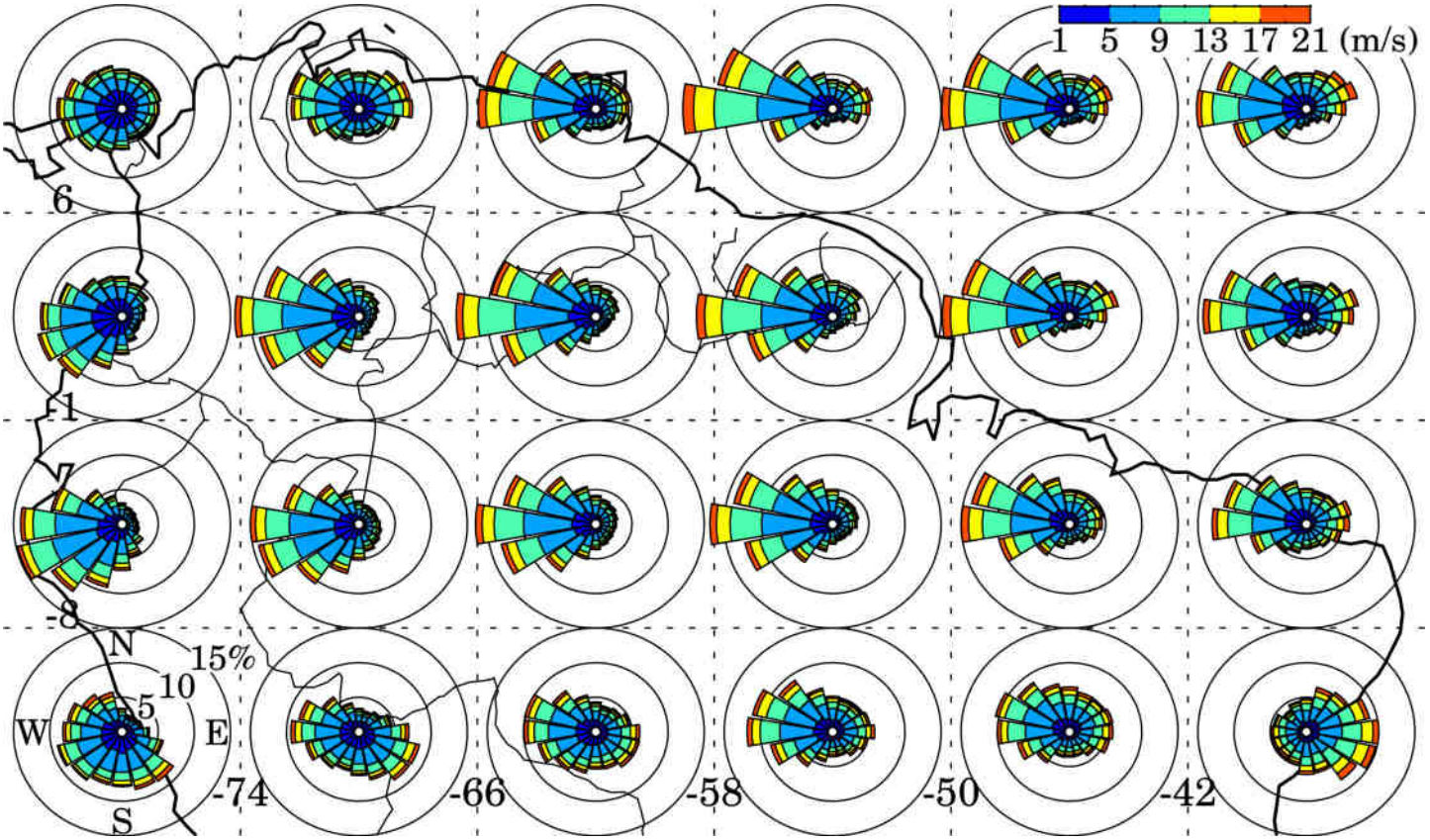

Figure 7. Regional convective systems velocities wind rose every 7° × 8°.

approximately 30% of all systems velocities, even though, between 74° W – 66° W and 8° S – 6° N we observed the lower amount (≈ 20%) of eastward propagation components. The sub-regions (7° × 8°) over the Atlantic Ocean presented northeastward propagation sectors that exceed 5% of probability that must be partially associated with off shore convective propagation as shown by *Negri et al.* [1994].

On Amazon, the westward is the most probable propagation sector. The sectors with northwestward and southwestward components of velocity is very symmetric but, in North Hemisphere and South Hemisphere sub-regions, the sectors with northwestward and southwestward components has a little more occurrence respectively. Between 82° W – 34° W and 15° S – 8° S, also between 82° W – 74° W and 6° N – 13° N there is no westward predominant propagation of systems. These are the regions where the propagation directions of systems are most aleatory.

In general 4 different propagations behaviors can be identified. One over the ocean with the most dominant westward propagation. The Central Amazonas sector very similar around all the region with also a predominant westward propagation with a larger dispersion in the direction of propagations. There are the system close/over the Andes with a much less predominance of westward, in the north there is no predominant direction of propagation. Finally, the south of Amazonas, where middle latitudes system moves north-eastward and combined with the local Amazonas convective systems reduces the westward probability. The region most southeast has a predominant eastward propagation, probably related to the cold fronts incursions in this region moving to northeast.

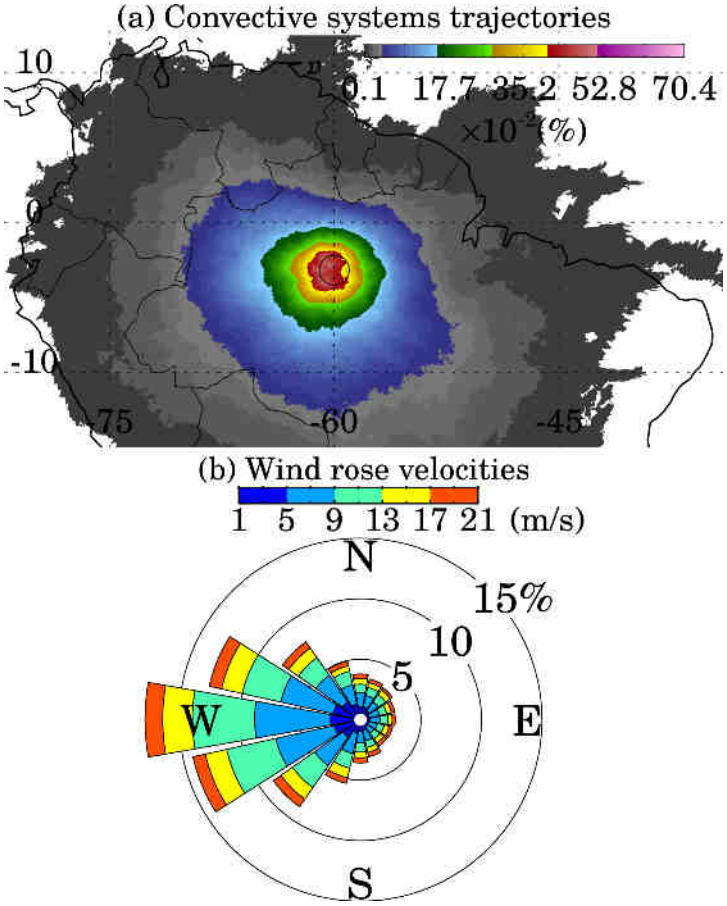

Figure 8. Geographic density of convective systems trajectories (a) and wind rose of convective systems velocities (b) just for systems that crossed the SIPAM radar range during GoAmazon2014/15.

These propagations velocities distribution revel the diversity of the Amazon convection. For example, interesting features can be observed selecting the 1926 convective systems that moved, at least one time, over the Manaus SIPAM radar range during the GoAmazon 2014/15. The figure 8 shows, the geographic probability density of these trajectories and the velocity wind rose distribution with same bin sizes and velocities limits (between 1 m/s and 21 m/s) as in Fig. 7. One can note that the systems trajectories in figure 8a, have not a preferential path to overpass Manaus, but, cover all Amazon region and adjacencies. In figure 8b the most probable velocity is 18% in westward direction sector, same direction as the average for Central Amazonia described by *Rehbein et al.* [2017]; *Laurent et al.* [2002, Fig. 5], though, the 82% remaining are in different sectors from the average. Similarly, as in figure 6, the figure 8b revel 24% of the velocities in sectors where there is eastward zonal propagation and, 49% and 51% of velocities in sectors with northward and southward meridional propagation respectively.

3.3 Genesis, propagation and dissipation

To brings up an idea of where is the position that the genesis (t_i) and dissipation (t_f) were more often inside the Amazon region during 2014 and 2015, we selected just the systems with at least 2 hours and 30 minutes to guarantee an amount of 5 cloud clusters or more, a total of 42,527 systems. Then, we selected 5 times with the same lifetime fraction in each system: t_i, t_1, t_2, t_3, and t_f. Beyond of the t_i and t_f we have three steps of time associate with the propagation of systems. The positions of genesis and dissipation have not considerable change by

season, but we need to have in mind that in accordance with the season, in some places the systems are more frequent as showed in figure 5.

In figure 9 is shown all cloud clusters areas gridded of each system in each time (t_i, t_1, t_2, t_3, and t_f) normalized by each lifetime. The probability values in percentage distributed geographically in each $0.04^\circ \times 0.04^\circ$ are referent of the total of 42,527 systems.

In general there is an expansion of clusters areas since the genesis until t_2, when the most of convective systems reaches the maturity, and after a decrease of clusters areas until the dissipation. For example the area with values above of 0.282% of probability of occurrence (above of 120 systems occurred) is larger in t_2 because generally in this time the systems reaches the maximum area, and we have more overlaps of clusters from different systems. In genesis and dissipation its areas are shorter and the highest probabilities values are concentrated in shorter geographical regions.

With respect to the coastal systems, mainly in Guyana, Surimane, French Guiana, and Amapa, the genesis (figure 9a) and dissipation (figure 9e) is not clearly identified because the initial and final areas of these systems are small. But when we look for figures 9b, 9c and 9d in the probabilities values around 0.127%, the propagation steps clearly shows systems that start on coast, probably associated with the sea breeze, with a propagation around 100 km inland and after dissipate.

The coastal genesis in Brazilians States of Para and Maranhão are more clearly observed in figure 9a. In Para, the coastal systems has genesis more often in Ilha de Marajo, and we can observe that along the Tocantins River basin the genesis also are often. The more often positions of dissipation (figure 9e) associated with the coastal systems in Para and Maranhão has probabilities values between 0.127% and 0.200%, some tens of kilometers of coastline.

In Para State, mainly in figure 9c and 9d, probabilities around 0.310% are found between of Terra Indígena Parakanã region, city of Bom Jesus do Tocantis and Rondon do Pará, that are localized beside of a large portion of Tocantins River. Another region after of coast and associate with large amount of genesis and also with the increase of systems areas in Para, mainly in figures 9a, 9b, and 9c is observed between the Terra Indígena Zo'é and Floresta Nacional Saracá-Taquera in region of Oriximiná and Óbidos cities.

On days with coastal squall lines similar to those observed by *Kousky* [1980]; *Garstang et al.* [1994]; *Cohen et al.* [1995]; *Rickenbach* [2004], sometimes we observed systems with clear coastal formation, with large areas (e.g., 10^4 km^2) close to the coast, but in other times exhibit weak cloudiness near to coast and only it develops when reaches the Central Amazon Basin and make merge with the local convection. The regions in Para with high geneses probabilities after of coast, can promote new systems that make merge with cloudiness from coast, and these mergers make it difficult to distinguish between basin systems and coastal systems if you try realize a classification as done by *Greco et al.* [1990].

After the coastal region and more inside the Amazon Basin, in figure 9a the region with probabilities between 0.127% and 0.251% is very big, indicating that all Central Amazon Basin region is a place of genesis. We can observe some higher probabilities values associate with higher topography as the region of Pico da Neblina in frontier between Brazil and Venezuela and region of Canaima and Jaua-Sarisariama National Parks in Venezuela. On the other hand, regions with altitude practically in the same as the sea level has probabilities of genesis very close with the places with high topography, around 0.210%, showing that the geneses is not localized specially in places with higher topography. The diurnal forcing and local circulation as rivers breezes, act promoting this environment of systems geneses quite homogeneous.

The color bars in figure 9 shows values until 0.500%, but in extreme North of Andes mountain range, and region of Colombia, Venezuela, Panama and adjacent Pacific Ocean, the maximum probabilities reached 0.804%.

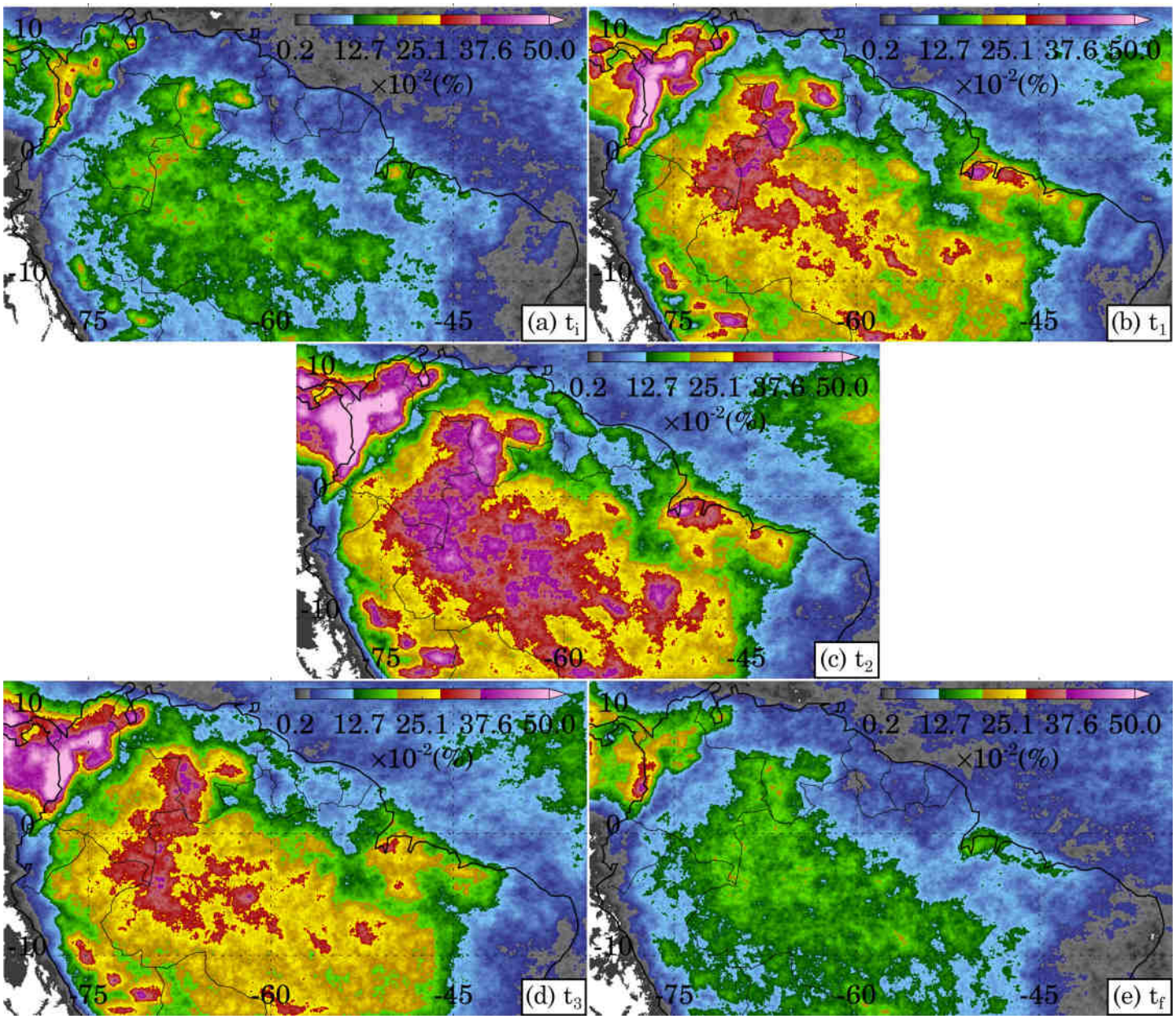

306 **Figure 9.** Lifetime normalized in 5 times: t_i, t_1, t_2, t_3 and t_f. The maps show the convective systems cloud
307 clusters areas probability of occurrence in each normalized time. Just systems with at least 2 hours and 30
308 minutes are selected.

4 Conclusions

With the convective systems trajectories defined based on cloud clusters (Tb $\leq$ 235 K) areas, have been made high resolution maps with new details about the geographic density of trajectories and places where the genesis, propagation and dissipate are most frequent in Amazonia.

Although the average of systems velocities [*Rehbein et al.*, 2017; *Laurent et al.*, 2002] indicate westward predominant displacements for Amazonian convective systems, a larger dispersion in the direction of propagations is found as by PDF and CDF (Fig. 6) as well by the wind rose convective systems velocities plots (Fig. 7). The westward Amazonian convective systems propagation velocity sector in figure 7 corresponds to 18–15%, while the remaining are distributed in others sectors.

The total sample of systems velocities (Fig. 6) shows practically the same probability of meridional velocities northward or southward and 35% of sampling of zonal velocities are associated with eastward movement. Velocities in Andes has less predominance of westward and in region of extreme north of Andes, there is no predominant convective system velocity propagation direction. In extreme southeast of study area, there is predominant eastward propagation velocity, probably related to the cold fronts incursions.

All Central Amazon Basin region is a quite homogeneous place of convective systems geneses. Some higher probabilities values associate with higher topography as Pico da Neblina, National Parks Canaima and Jaua-Sarisariñama are observed, but regions practically in the sea level has probabilities of genesis very close with the places with high topography, showing that the geneses is not localized specially in places with higher topography, but the local circulation as rivers breezes, act as a component of geneses as important as the topography.

The occurrence of coastal and basin convective systems has a seasonal dependence. During SON, the convective systems are more often in central part of Amazon Basin while during MAM the trajectories are more connected between the coastal region and the Central Amazon Basin. The coastal convective systems from Para and Maranhão are more often than the coastal convective systems from the north side of Amazon River (Amapa, French Guiana, Suriname and Guyana).

The top 10% of trajectories and lifetimes, that is to say, the extreme events, has areas between 7.68921×10^4 km^2 and 5.2476340×10^6 km^2 and lifetimes between 7 h and 82 h.

Studying just the tracks that across the SIPAM radar range that participated of GoAmazon 2014/15, we cannot see any preferable propagation path for the systems that reaches the Manaus city region, localized practically in the center of Amazonia. Coastal systems that reached the SIPAM radar range as shown in Fig. 8a, had probability of occurrence around 0.001 – 0.01 %, i.e. approximately 1–12 systems in 2 years. In *Alcântara et al.* [2011] using *Cohen* [1989] ACSL classification made visually per infrared geostationary images, was found ≈35 ACSL per year with more than 400 km of inland propagation. To reach Manaus, a system must travel more than 1000 km and in this study, independent of systems be classified as ACLS, just in the maximum 6 per year are long-lived enough to travel from coast to Manaus.

The propagation of cloud clusters from coast to Manaus region mainly during MAM can be seen in *Garreaud and Wallace* [1997]; *Burleyson et al.* [2016]. Alternatively, the cloud clusters positions normalized by the lifetime (fig. 9), not revel a march of thousands of kilometers from coast to Central Amazonia, even if separated just the MAM period (figure not shown), but shows coastal systems with some tens of kilometers of propagation inland, probably associate with the act of sea breeze. Cloudiness that travel from coast by hundreds or thousands of kilometers, rarely are one system with coastal genesis and dissipation in Central Amazonia, but are a composition of several systems with different genesis and dissipation position during the path from coast to central region. The march of cloud clusters from coast to Cen-

tral Amazonia must have the influence of another mechanism beyond the sea breeze as the low level jet describe by *Alcântara et al.* [2011]; *Cohen et al.* [1995].

The convective systems tracking by successive geostationary infrared images is revisited in this research. We could verify that situations wherein merge, split, and continuity occurs simultaneously, named with multiple process, participated in 10% of total valid connection between cloud clusters in t_0 and t_0+dt. In previous studies that made systems tracking over Amazon region selected just those systems with spontaneous genesis and dissipation by simple decay, but in this research all systems tracked are shown. Complexes merge and spits, as well as multiple processes are frequent and can promote big changes in cloud cluster geometric center and this is the realist behavior of convection even if this promotes very big displacements. Considering methods of nowcasting based on systems tracking, a study as has been presented in Fig. 7, can supply statistic data to improve the assertiveness of systems expected velocity, manly when very big displacements precedes the timing of forecast.

Acknowledgments

The CAPES Foundation grant 99999.000481/2016-05 by the financial support.

References

Alcântara, C. R., M. A. S. Dias, E. P. Souza, and J. C. Cohen (2011), Verification of the role of the low level jets in amazon squall lines, *Atmospheric Research*, *100*(1), 36–44.

Angelis, C. F., G. R. McGregor, and C. Kidd (2004), A 3 year climatology of rainfall characteristics over tropical and subtropical south america based on tropical rainfall measuring mission precipitation radar data, *International Journal of Climatology: A Journal of the Royal Meteorological Society*, *24*(3), 385–399, doi:10.1002/joc.998.

Burleyson, C. D., Z. Feng, S. M. Hagos, J. Fast, L. A. Machado, and S. T. Martin (2016), Spatial variability of the background diurnal cycle of deep convection around the goamazon2014/5 field campaign sites, *Journal of Applied Meteorology and Climatology*, *55*(7), 1579–1598.

Chambon, P., R. Roca, I. Jobard, and J. Aublanc (2012), The tapeer-brain product: Algorithm theoretical basis document, level 4, *Megha-Tropiques Tech. Memo*, *4*, 13.

Chambon, P., I. Jobard, R. Roca, and N. Viltard (2013), An investigation of the error budget of tropical rainfall accumulation derived from merged passive microwave and infrared satellite measurements, *Quarterly Journal of the Royal Meteorological Society*, *139*(673), 879–893.

Chen, S. S., R. A. Houze Jr, and B. E. Mapes (1996), Multiscale variability of deep convection in realation to large-scale circulation in toga coare, *Journal of the Atmospheric Sciences*, *53*(10), 1380–1409.

Cohen, J. C., M. A. Silva Dias, and C. A. Nobre (1995), Environmental conditions associated with amazonian squall lines: A case study, *Monthly Weather Review*, *123*(11), 3163–3174.

Cohen, J. C. P. (1989), An observational study of amazon squall lines (in portuguese), Master's thesis, Institute for Space Research, Sao Jose dos Campos – Brazil.

Garreaud, R., and J. M. Wallace (1997), The diurnal march of convective cloudiness over the americas, *Monthly Weather Review*, *125*(12), 3157–3171.

Garstang, M., H. L. Massie Jr, J. Halverson, S. Greco, and J. Scala (1994), Amazon coastal squall lines. part i: Structure and kinematics, *Monthly Weather Review*, *122*(4), 608–622.

Greco, S., R. Swap, M. Garstang, S. Ulanski, M. Shipham, R. Harriss, R. Talbot, M. Andreae, and P. Artaxo (1990), Rainfall and surface kinematic conditions over central amazonia during able 2b, *Journal of Geophysical Research: Atmospheres*, *95*(D10), 17,001–17,014.

Horel, J. D., A. N. Hahmann, and J. E. Geisler (1989), An investigation of the annual cycle of convective activity over the tropical americas, *Journal of Climate*, *2*(11), 1388–1403.

Houze Jr, R. (1993), Cloud dynamics, 573 pp, *Academic, San Diego, Calif.*

Kousky, V. E. (1980), Diurnal rainfall variation in northeast brazil, *Monthly Weather Review*, *108*(4), 488–498.

Laurent, H., L. A. Machado, C. A. Morales, and L. Durieux (2002), Characteristics of the amazonian mesoscale convective systems observed from satellite and radar during the wetamc/lba experiment, *Journal of Geophysical Research: Atmospheres*, *107*(D20).

Machado, L., W. Rossow, R. Guedes, and A. Walker (1998), Life cycle variations of mesoscale convective systems over the americas, *Monthly Weather Review*, *126*(6), 1630–1654.

Machado, L., H. Laurent, N. Dessay, and I. Miranda (2004), Seasonal and diurnal variability of convection over the amazonia: a comparison of different vegetation types and large scale forcing, *Theoretical and Applied Climatology*, *78*(1), 61–77.

Machado, L. A. T., and H. Laurent (2004), The convective system area expansion over amazonia and its relationships with convective system life duration and high-level wind divergence, *Monthly Weather Review*, *132*(3), 714–725.

Martin, S. T., P. Artaxo, L. Machado, A. Manzi, R. Souza, C. Schumacher, J. Wang, M. Andreae, H. Barbosa, J. Fan, et al. (2016), Introduction: observations and modeling of the green ocean amazon (goamazon2014/5), *Atmospheric Chemistry and Physics*, *16*(8), 4785–4797.

Mathon, V., and H. Laurent (2001), Life cycle of sahelian mesoscale convective cloud systems, *Quarterly Journal of the Royal Meteorological Society*, *127*(572), 377–406.

Negri, A. J., R. F. Adler, E. J. Nelkin, and G. J. Huffman (1994), Regional rainfall climatologies derived from special sensor microwave imager (ssm/i) data, *Bulletin of the American Meteorological Society*, *75*(7), 1165–1182, doi:10.1175/1520-0477(1994)075¡1165:RRCDFS¿2.0.CO;2.

Rehbein, A., T. Ambrizzi, and C. R. Mechoso (2017), Mesoscale convective systems over the amazon basin. part i: climatological aspects, *International Journal of Climatology*.

Rickenbach, T. M. (2004), Nocturnal cloud systems and the diurnal variation of clouds and rainfall in southwestern amazonia, *Monthly Weather Review*, *132*(5), 1201–1219.

Roca, R., P. Chambon, I. Jobard, P.-E. Kirstetter, M. Gosset, and J. C. Bergès (2010), Comparing satellite and surface rainfall products over west africa at meteorologically relevant scales during the amma campaign using error estimates, *Journal of Applied Meteorology and Climatology*, *49*(4), 715–731.

Santos, M. J., M. A. F. Silva Dias, and E. D. Freitas (2014), Influence of local circulations on wind, moisture, and precipitation close to manaus city, amazon region, brazil, *Journal of Geophysical Research: Atmospheres*, *119*(23), 13,233–13,249, doi:10.1002/2014JD021969.

Tang, S., S. Xie, Y. Zhang, M. Zhang, C. Schumacher, H. Upton, M. P. Jensen, K. L. Johnson, M. Wang, M. Ahlgrimm, et al. (2016), Large-scale vertical velocity, diabatic heating and drying profiles associated with seasonal and diurnal variations of convective systems observed in the goamazon2014/5 experiment, *Atmospheric Chemistry and Physics*, *16*(22), 14,249.

Vila, D. A., L. A. T. Machado, H. Laurent, and I. Velasco (2008), Forecast and tracking the evolution of cloud clusters (fortracc) using satellite infrared imagery: Methodology and validation, *Weather and Forecasting*, *23*(2), 233–245.

Williams, M., and R. A. Houze Jr (1987), Satellite-observed characteristics of winter monsoon cloud clusters, *Monthly Weather Review*, *115*(2), 505–519.

Woodley, W. L., C. G. Griffith, J. S. Griffin, and S. C. Stromatt (1980), The inference of gate convective rainfall from sms-1 imagery, *Journal of Applied Meteorology*, *19*(4), 388–408.